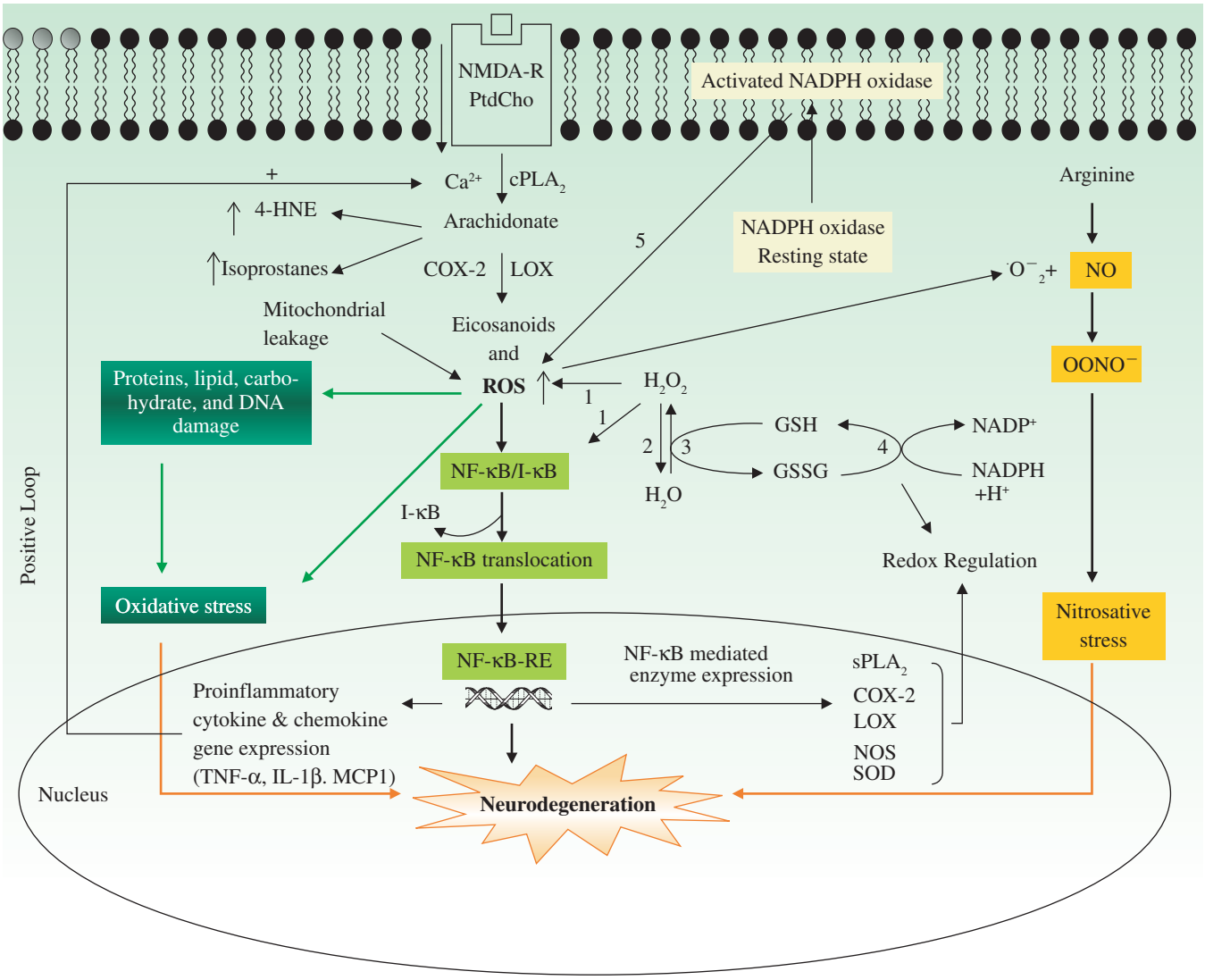

Fig. 1.2 Generation of reactive oxygen species (ROS) and enzymic and nonenzymic markers for oxidative stress. 1, Superoxide dismutase (SOD); 2, catalase; 3, glutathione peroxidase; 4, glutathione reductase; 5, NADPH oxidase. $cPLA_2$, cytosolic phospholipase A_2; $sPLA_2$, secretory phospholipase A_2; COX-2, cyclooxygenase-2; LOX, lipoxygenase; NOS, nitric oxide synthase; GSH, reduced glutathione; GSSG, oxidized glutathione; H_2O_2, hydrogen peroxide; 4-HNE, 4-hydroxynonenal; NO, nitric oxide; $OONO^-$, peroxynitrite. Activation of NF-κB by ROS leads to its translocation to the nucleus, where it facilitates the transcription of proinflammatory enzymes ($sPLA_2$, COX-2, NOS, and SOD) and proinflammatory cytokines (TNF-α and IL-1β). These cytokines upregulate activities of $cPLA_2$ and $sPLA_2$ through a positive loop mechanism in cytoplasm and neural membranes. Upward arrows indicate increase in levels of metabolites.

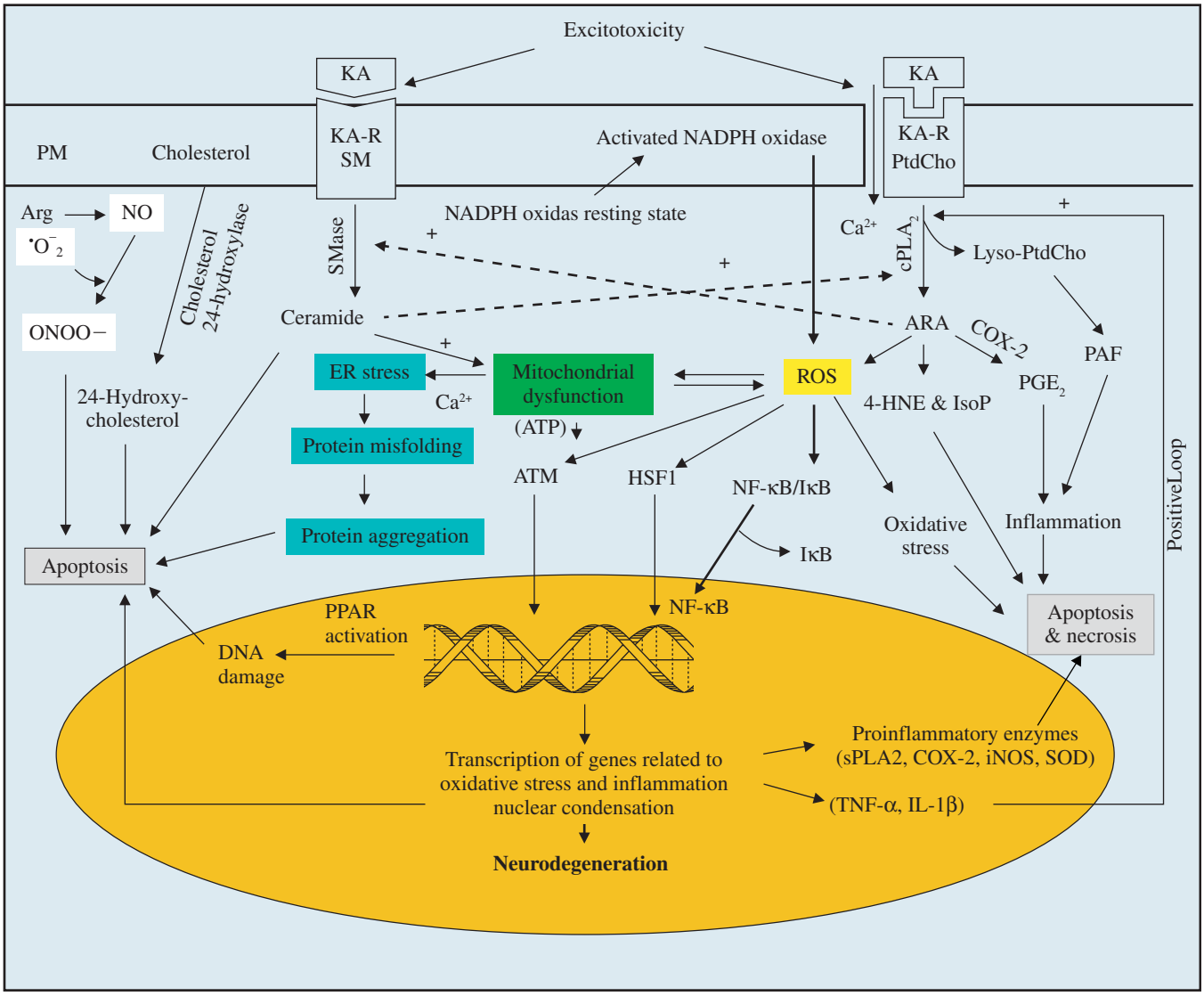

Fig. 4.4 Diagram showing interactions between glycerophospholipid and sphingolipid lipid-derived lipid mediators. KA, kainate; KA-R, kainate receptor; SM, sphingomyelin; SMase, sphingomyelinase; cPLA$_2$, cytosolic phospholipase A$_2$; PtdCho, phosphatidylcholine; ARA, arachidonic acid; Lyso-PtdCho, lyso-phosphatidylcholine; sPLA$_2$, secretory phospholipase A$_2$; COX-2, cyclooxygenase-2; iNOS, inducible nitric oxide synthase; ROS, reactive oxygen species; SOD, superoxide dismutase; 4-HNE, 4-hydroxynonenal; PGE$_2$, prostaglandin E$_2$; PAF, platelet-activating factor; IsoP, isoprostane; Arg, L-arginine; NO, nitric oxide; ONOO^{-}, peroxynitrite; NF-κB, nuclear factor-κB; TNF-α, tumor necrosis factor-α; IL-1β, interleukin-1β; PARP, poly(ADP-ribose) polymerase; ATM, Ataxia-telangectasia mutated; HSF-1, heat shock transcription factor 1. Positive sign (+) indicates stimulation.

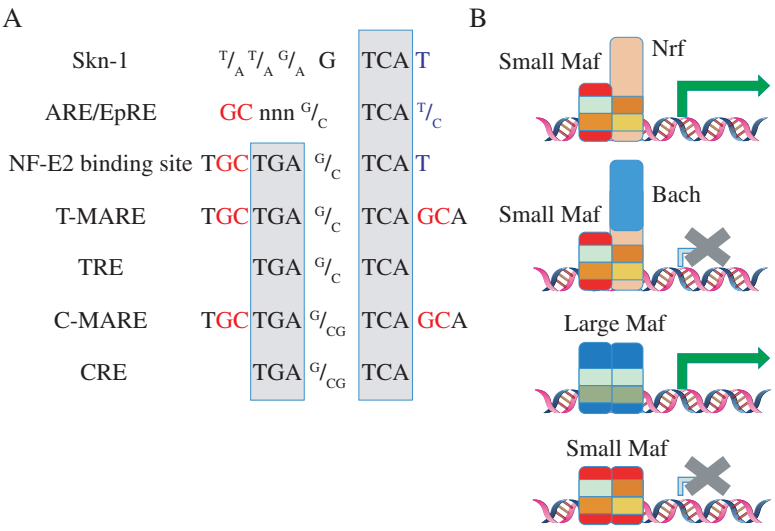

Fig. 5.2 DNA recognition sequences and the transcriptional activities of Maf-containing dimers. (A) Various MARE-related sequences are shown. The dinucleotide "GC" (marked in red) is essential for recognition by Maf proteins. The nucleotide "T" or "T/C" (marked in blue) enhances the binding of CNC proteins. Trinucleotides (boxed in gray) with the central G and GC sequence consist of the TRE and CRE, respectively, which make up the core region of the MARE. (B) Nrf1, Nrf2, Nrf3, and NF-E2 activate transcription by forming heterodimers with small Maf, while Bach1 and Bach2 repress transcription. A large Maf homodimer, possessing a *trans*-activation domain, activates transcription, while a small Maf homodimer, lacking a *trans*-activation domain, represses transcription. All of these Maf-containing dimers bind to T-MARE with high affinity.

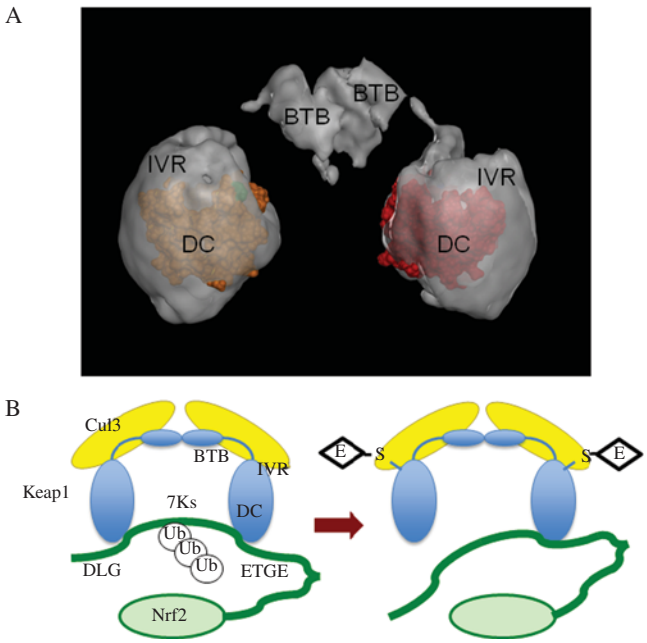

Fig. 5.6 The overall structure of the Keap1 homodimer and the regulation of Nrf2 activity by Keap1. (A) The three-dimensional structure of the Keap1 homodimer (cited from Ogura et al., *Proc Natl Acad Sci USA*. 2010:2842-7, 107). (B) Interaction between Nrf2 and the Keap1-Cul3 complex under unstressed conditions (left) and stressed conditions in which thiols are modified with electrophiles (E) (right). Each DC domain of the Keap1 homodimer binds to the DLG and ETGE motifs in the Neh2 domain of Nrf2. Keap1 is proposed to interact with Cul3 at the BTB domain and the IVR. Nrf2 is polyubiquitinated at 7 lysine residues (7Ks) between the DLG and ETGE motifs (left). Modification of Keap1 with electrophiles is thought to alter the overall conformation of the Keap1-Cul3 and Nrf2 complex, which inhibits Nrf2 ubiquitination (right).

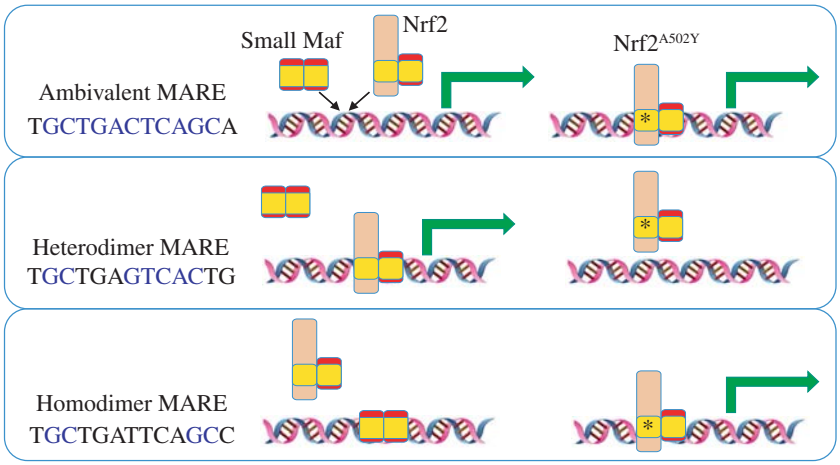

Fig. 5.8 Categorization of MARE-related sequences. Ambivalent MAREs are bound by both Nrf2-small Maf heterodimers and Maf homodimers. Heterodimer MAREs are preferentially bound by Nrf2-small Maf heterodimers, and homodimer MAREs are bound by Maf homodimers. Substitution of the alanine residue of the Nrf2 basic region with a tyrosine residue switches the DNA recognition specificity from the CNC type to the Maf type and results in the preferential binding of Nrf2 A502Y-small Maf heterodimers to homodimer MAREs and not to heterodimer MAREs.

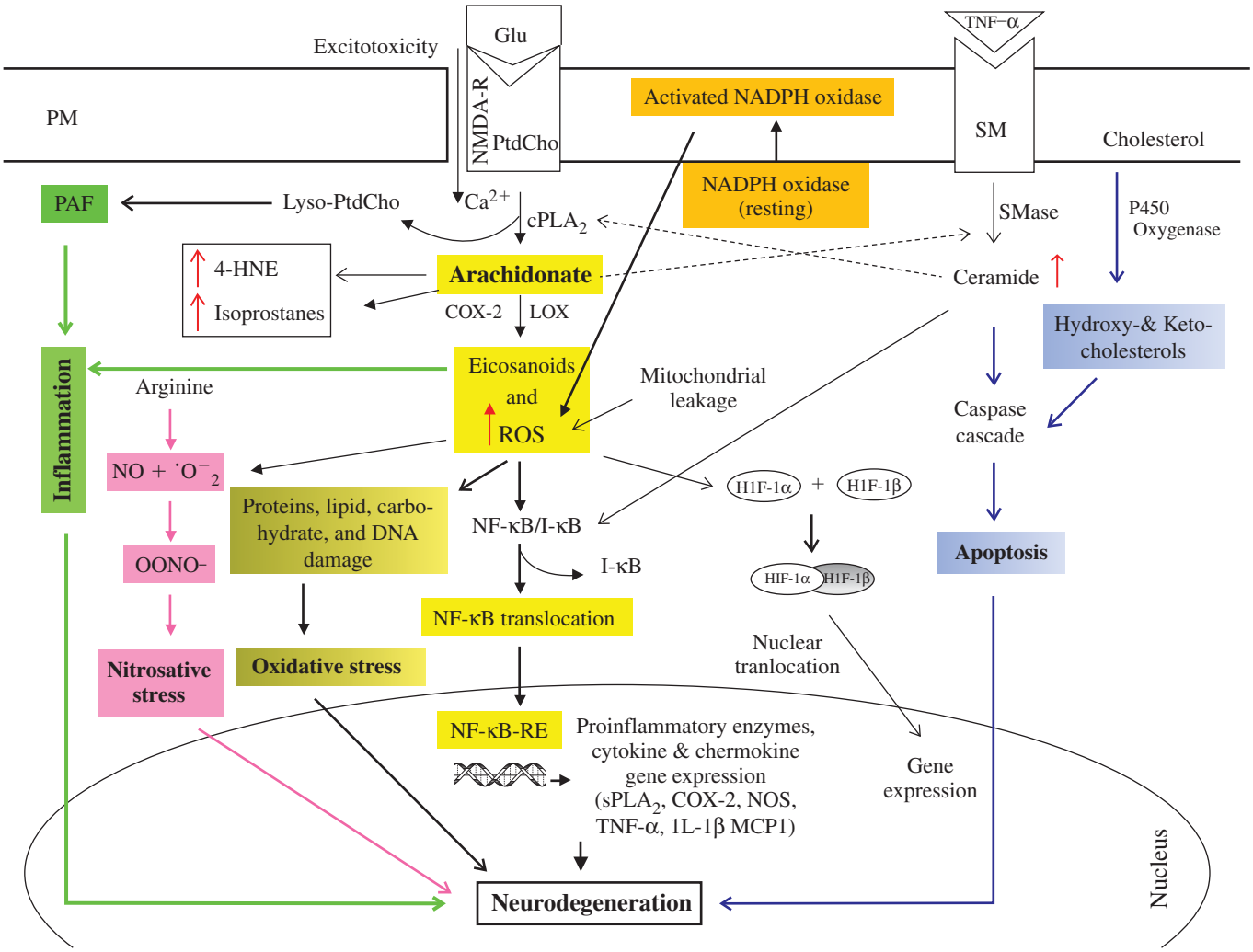

Fig. 7.3 Generation of lipid mediators and interactions between excitotoxicity, oxidative stress, and neuroinflammation in neurodegenerative diseases. $cPLA_2$, cytosolic phospholipase A_2; $sPLA_2$, secretory phospholipase A_2; COX-2, cyclooxygenase-2, LOX, lipoxygenase; NOS, nitric oxide synthase; SMase, sphingomyelinase; TNF-α, tumor necrosis factor-α; IL-1β, interleukin 1β; lyso-PtdCho, lyso-phosphatidylcholine; ROS, reactive oxygen species; HIF-1, hypoxia-inducible factor-1; 4-HNE, 4-hydroxynonenal; NO, nitric oxide; $OONO^{-}$, peroxynitrite; PAF, platelet-activating factor. Activation of NF-κB by ROS leads to its translocation to the nucleus, where it facilitates the transcription of proinflammatory enzymes ($sPLA_2$, COX-2, NOS, and SOD) and proinflammatory cytokines (TNF-α and IL-1β). These cytokines upregulate activities of $cPLA_2$ and $sPLA_2$ through a positive loop mechanism in cytoplasm and neural membranes. Upward arrows indicate increase in levels of metabolites.

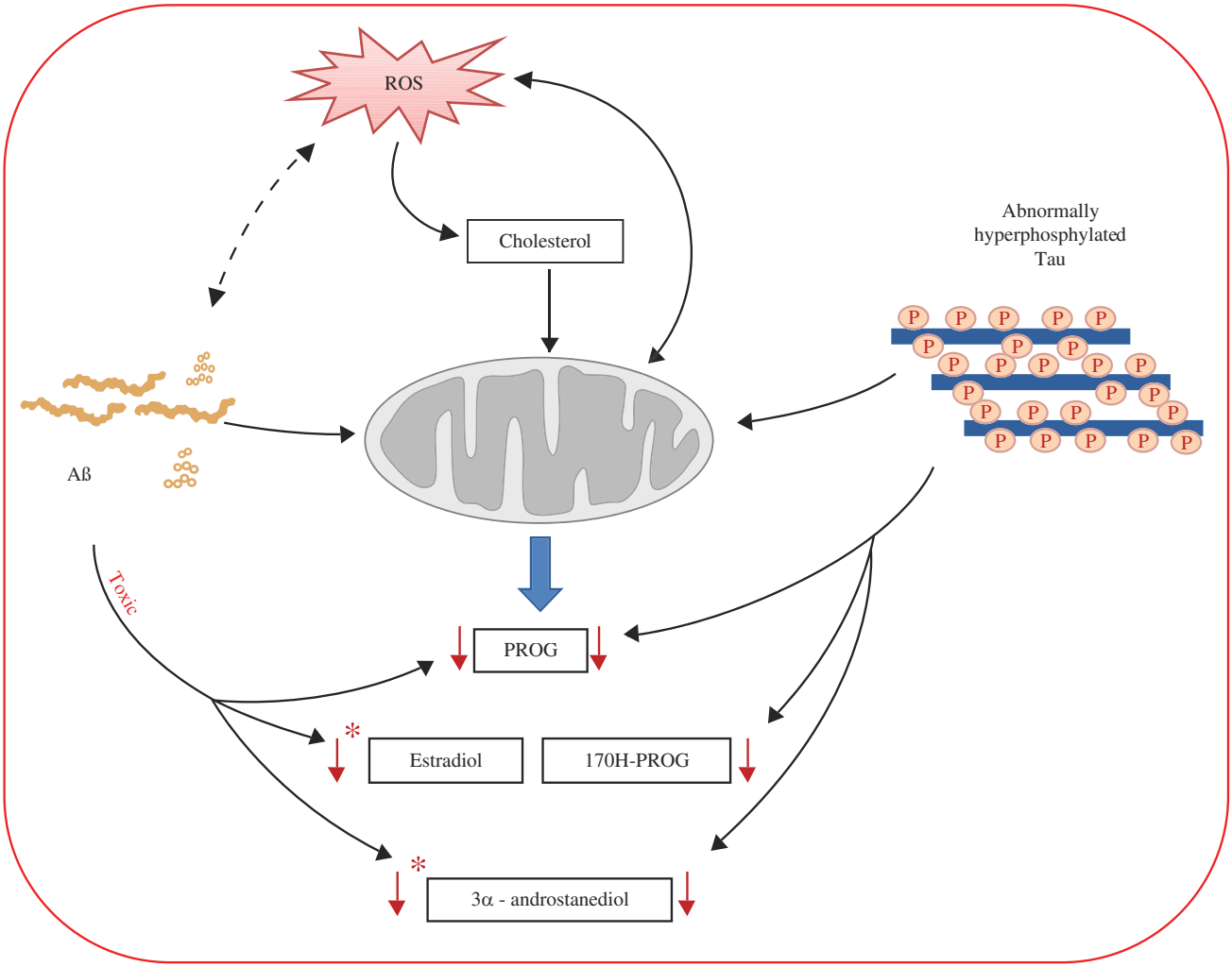

Fig. 8.3 Effect of toxic concentrations of Aβ peptides and abnormally hyperphosphorylated Tau protein on neurosteroid biosynthesis. Aβ induced a drop of the level of progesterone (PROG), estradiol, and 3α-androstanediol by acting on reactive oxygen species (ROS) formation and mitochondrial function and/or directly on steroidogenesis. The presence of abnormally hyperphosphorylated Tau protein had the same effect by inducing a decrease of progesterone, 17-hydroxyprogesterone (17OH-PROG), and 3α-androstanediol. On the other hand, it has been shown that nontoxic concentrations of Aβ induced an increase in estradiol and 3α-androstanediol levels (this pathway is marked by *).

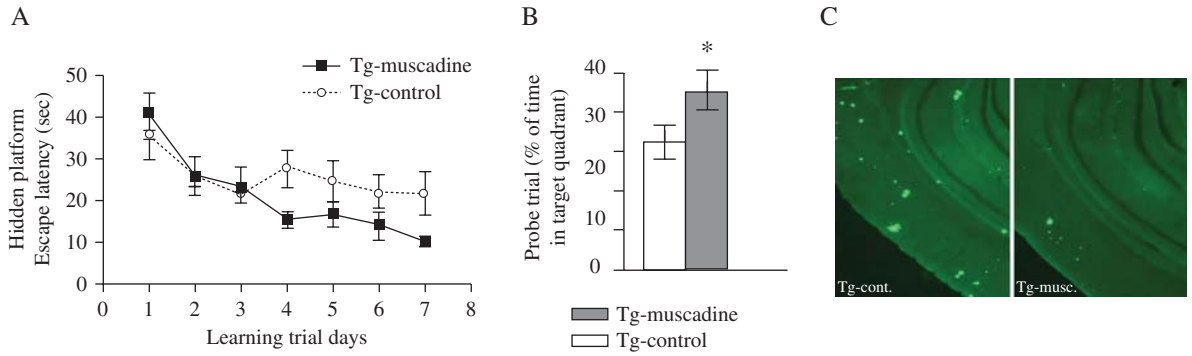

Fig. 16.4 Muscadine treatment improves spatial memory function and Aβ neuropathology in Tg2576 mice. (A,B) Assessments of spatial memory behavioral functions of 14 month old muscadine-treated (Tg-muscadine) and control, gender- and age-matched non-treated (Tg-control) Tg2576 mice using the Morris water maze protocol. (A) Learning trial hidden-platform acquisition curves. Tg-muscadine group performed significantly better than the control, non-treated group (Tg-control) [2-way ANOVA analysis of Tg-muscadine vs. Tg-control groups for muscadine treatment ($p < 0.05$, $F = 4.24$, DFn = 1, DFd = 84) and for training days ($p < 0.05$, $F = 6.43$, DFn = 6, Dfd = 84)]. (B) Probe trial conducted 24 hours after completion of hidden-platform training. Muscadine-treated Tg2576 mice exhibited a significantly higher preference for the target platform compared to control, non-treated Tg2576 mice ($p < 0.05$, 2-tailed Student t test). In (A,B) Values represent group mean (+SEM); $n = 7–9$ mice per group. (C) Assessments of Aβ neuropathology reflected by amyloid neuritic plaque density in cerebral cortex and in the hippocampal formation of brain specimens from muscadine-treated and control, non-treated Tg2576 mice. Representative micrograph of brain specimen stained for amyloid neuritic plaques in muscadine-treated (Tg-musc.) or in control, non-treated (Tg-cont.) Tg2576 mice.

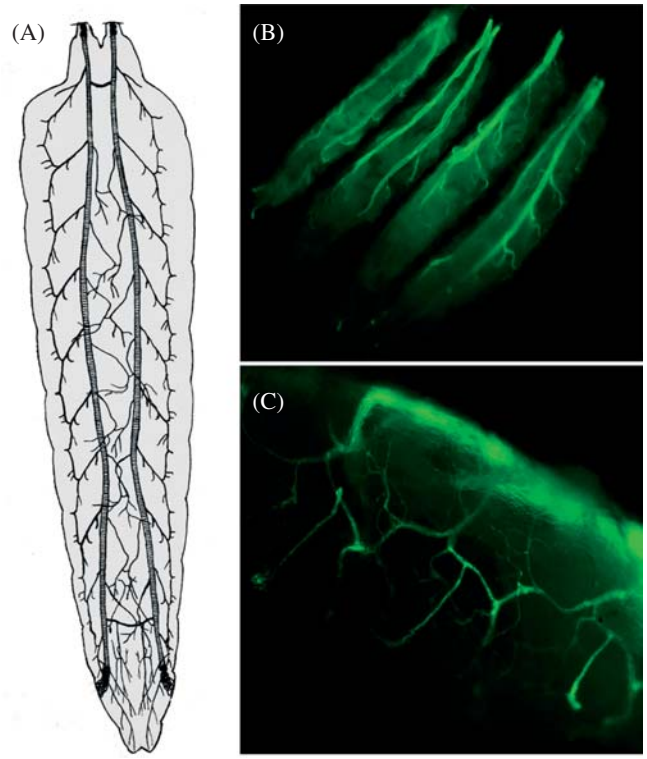

Fig. 19.2 Structure of the airway system of *Drosophila*. The airway system (trachea) of a larval fly is made up of interconnected tubes that deliver oxygen to almost every cell in the body (A). Upon stimulation with different stressors including infection, the airway epithelium launches a very effective response, comprising the expression of antimicrobial peptide genes (B and C, the latter at higher magnification).

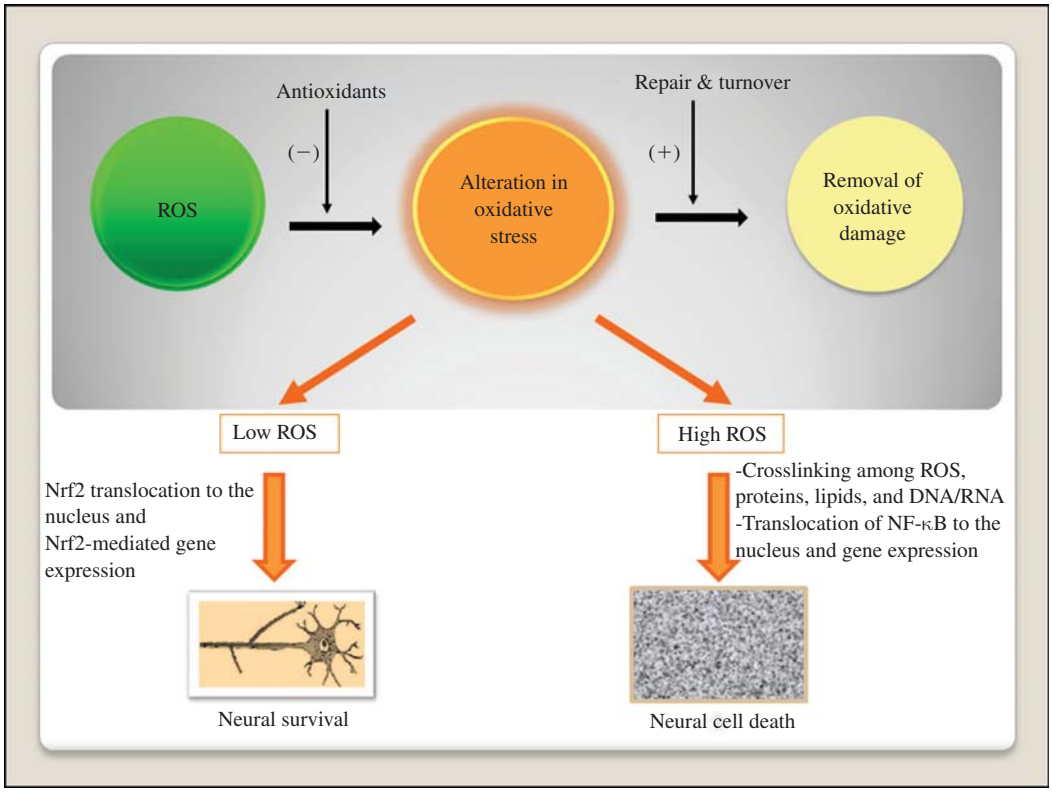

Fig. 21.2 Connection between reactive oxygen species (ROS)-mediated oxidative stress and abnormal functions. Increase in oxidant level, high ROS, decrease in antioxidants, and failure in repair and turnover result in functional abnormalities. Repair and turnover of oxidative damage, the so-called cellular defense mechanism, include DNA excision, resynthesis, and rejoining of DNA strands; repair of oxidized methionine residues in proteins; and normal membrane turnover releasing damaged lipids. Low ROS allow the translocation of nuclear factor-erythroid-2-related factor 2 (Nrf2) to the nucleus to regulate the expression of surviving genes for neural survival, whereas high ROS prevents translocation of Nrf2 to the nucleus. The cross-linking of high ROS occurs with proteins, lipids, DNA/RNA, which promotes neurodegeneration.

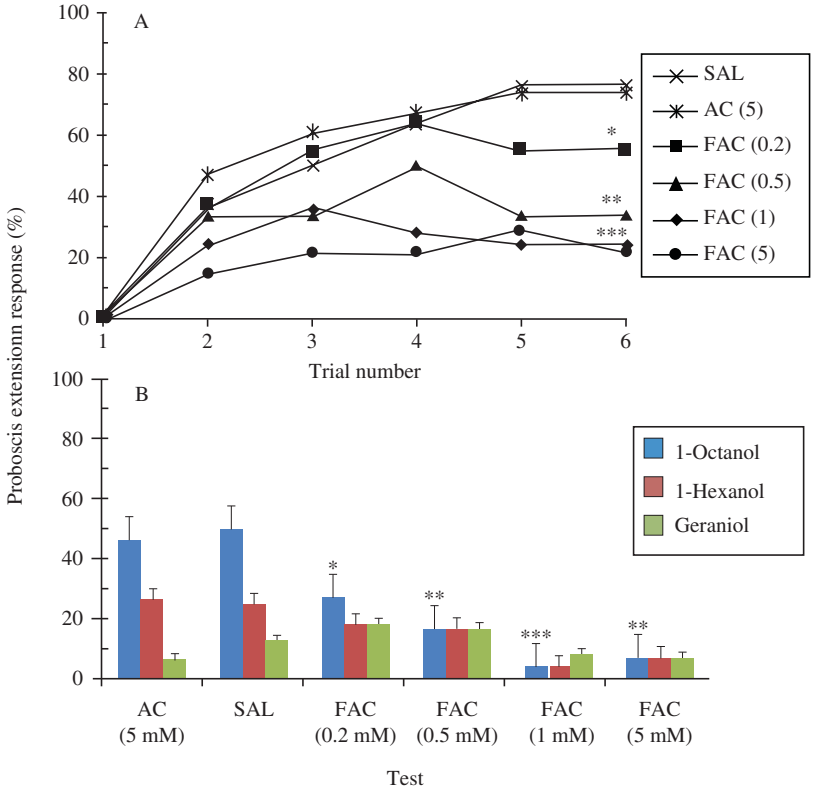

Fig. 21.3 Dose-response effect of ferrous ammonium citrate (FAC) on olfactory learning and memory. (A) Acquisition of the conditioned odor C: In this experiment, honeybees received 4 nl of saline (SAL), ammonium citrate (AC), or FAC at 0.2 mM, 0.5 mM, 1 mM, and 5 mM in each antennal lobe. Twenty-four hours later, subjects in each group were conditioned with 1-octanol (odor C). (B) Test with odors C, S, D: Ninety minutes after conditioning, subjects in each group were tested with C, molecularly similar (S), and molecularly dissimilar (D) odors in randomized order. *ns*, Not significantly different from controls (SAL, 5 mM AC). Asterisks indicate significant differences of respective points from control group: $*P = 0.05$, $**P = 0.005, 0.001$, $***P = 0.0001$). This figure is modified from reference [40].

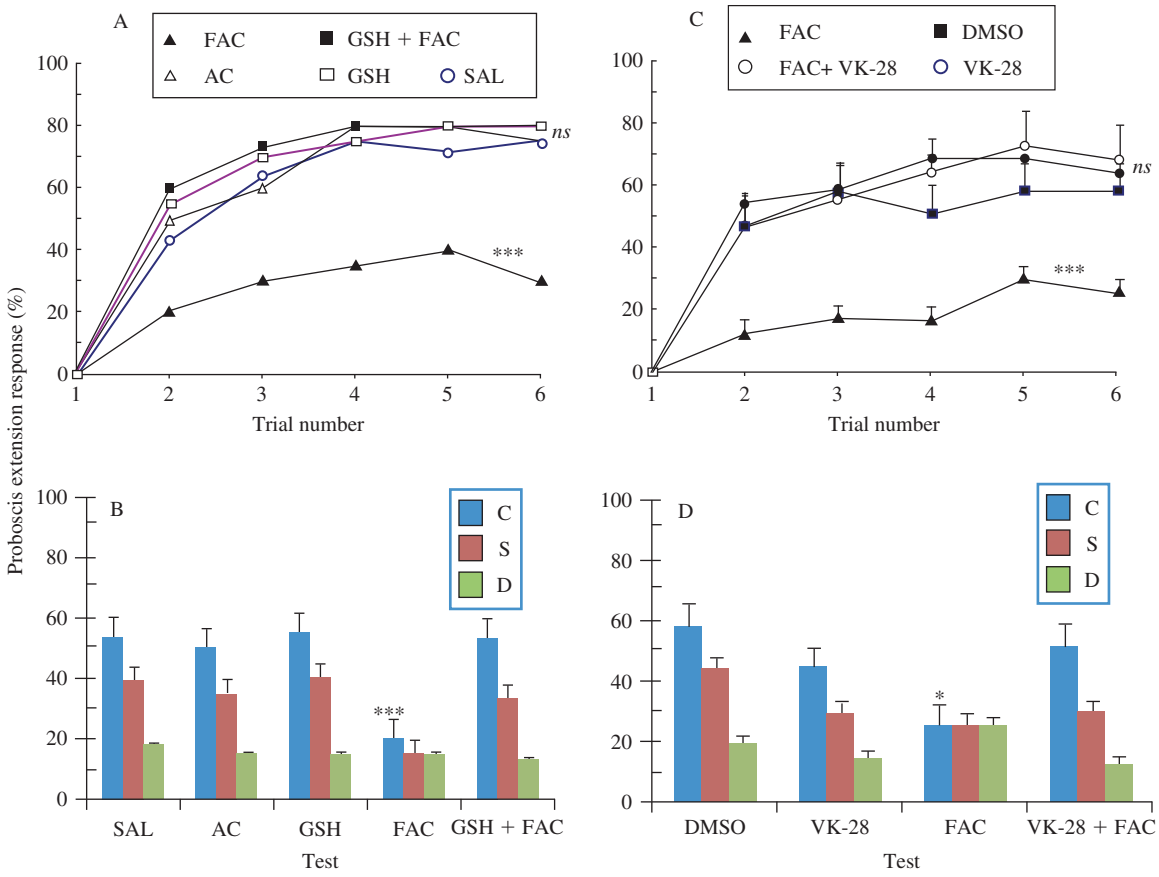

Fig. 21.4 Glutathione and VK-28 can reverse ferrous ammonium citrate (FAC)-mediated oxidative stress. (A) Acquisition of the conditioned odor C: In this experiment, subjects received 4 nl of either saline (SAL) or 2.5 mM reduced glutathione (GSH) in each antennal lobe. Two hours later, 4 nl of 500 μmol/l ammonium citrate (AC) or 500 μmol/l FAC were injected in each antennal lobe. Twenty-four hours later, subjects were conditioned with 1-octanol. (B) Test with odors C, S, D: Ninety minutes after conditioning, subjects in each group were tested with different odors (1-octanol, C; 1-hexanol, S; and geraniol, D) in randomized order. (C) Acquisition of the conditioned odor C: In this experiment, subjects received 4 nl of either dimethyl sulfoxide (DMSO) or VK-28 or DMSO + VK-28 in each antennal lobe 30 min before injection of FAC. Twenty-four hours later, subjects were conditioned with 1-octanol. (D) Test with odors C, S, D: Ninety minutes after conditioning, subjects in each group were tested with C, S, and D odors in randomized order. Asterisks indicate significant differences of respective points from control group (*$P = 0.05$, ***$P = 0.001$). *ns*, Not significant. This figure is modified from reference [40].

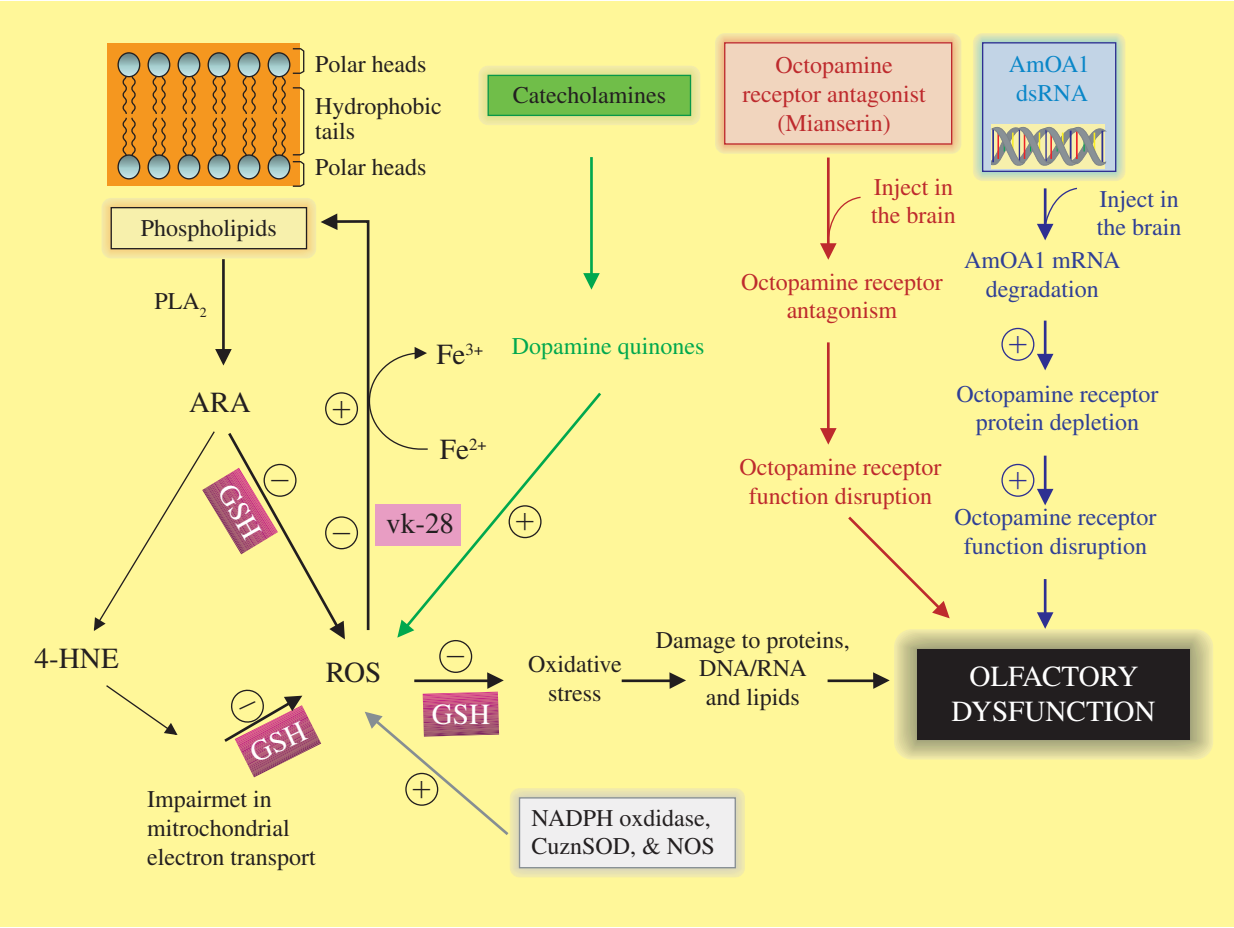

Fig. 21.5 Hypothetical molecular mechanism underlying reactive oxygen species (ROS)-mediated olfactory dysfunction in the honeybee brain. Iron-induced oxidative stress: Iron peroxidizes polyunsaturated fatty acids into peroxidized phospholipids, which are considered better substrates for phospholipase A_2 (PLA_2) than native phospholipids. PLA_2 catalyzes this reaction, forming arachidonic acid (ARA). The nonenzymatic oxidation of ARA results in the generation of 4-hydroxynonenal (4-HNE) that impairs mitochondrial electron transport, producing ROS. Increased ROS produces oxidative stress that damages proteins, DNA/RNA, and lipids, impairing olfactory processes (encoding, consolidation, and/or retrieval processes). Both octopamine receptor antagonism by mianserin (MAS) and octopamine receptor protein depletion by octopamine receptor double-stranded RNA (AmOA1-dsRNA) result in functional disruption of octopamine receptor, which leads to olfactory dysfunction. Oxidation of catecholamines forms quinones, which results in formation of ROS, leading to olfactory dysfunction. GSH protects brain against oxidative stress by modulating the redox state of specific thiol residues of target proteins. VK-28 chelates excess iron from the system. Monoamine oxidase inhibitor (MAOI) inhibits monamine oxidase enzyme and therefore prevents oxidation of catecholamines. ROS can also be produced by activation of NADPH oxidase.

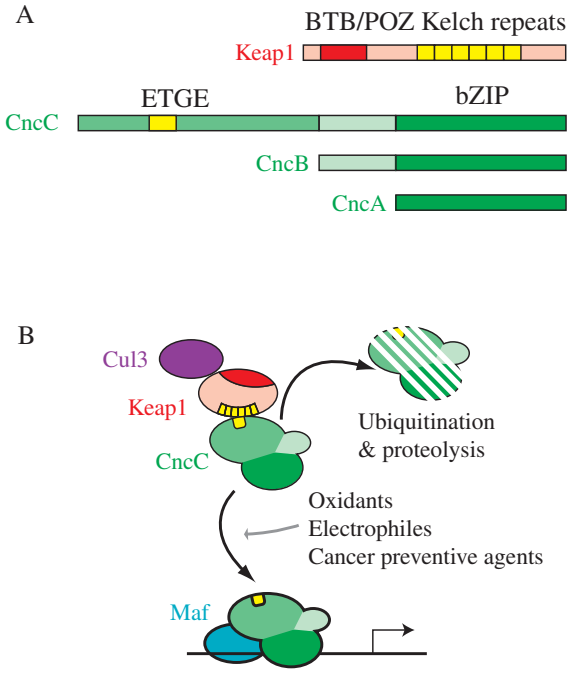

Fig. 22.1 Conservation and simplified illustration of the Keap1/Nrf2 pathway in *Drosophila*. (A) Nrf2 and Keap1 homologs are present in *Drosophila*. The fly *keap1* gene is predicted to encode a protein with high sequence similarity to its vertebrate Keap1 counterparts. Conserved domains include the BTB/POZ domain required for dimerization and 6 Kelch repeats for binding to Nrf2 and anchoring to actin. The *cnc* locus encodes three protein products, which all contain the bZIP region that mediates dimerization and DNA binding. The Nrf2 homolog is the longest isoform, CncC, which contains domains predicted to bind Keap1 such as the ETGE motif. (B) In basal conditions, Keap1 binds to CncC and inhibits its activity, likely through Cul3-mediated ubiquitination and proteasomal degradation. Oxidative stressors, electrophilic xenobiotics, and cancer chemopreventive agents relieve this inhibition. Stabilized CncC then accumulates in the nucleus and transcriptionally activates a battery of cell-protective genes, likely in a dimer with the single small Maf protein of *Drosophila*. This figure is adapted from Sykiotis GP and Bohmann D, Keap1/Nrf2 signaling regulates oxidative stress tolerance and lifespan in *Drosophila*, *Dev Cell*, vol. 14, p. 76–85, Copyright 2008, with permission from Elsevier.

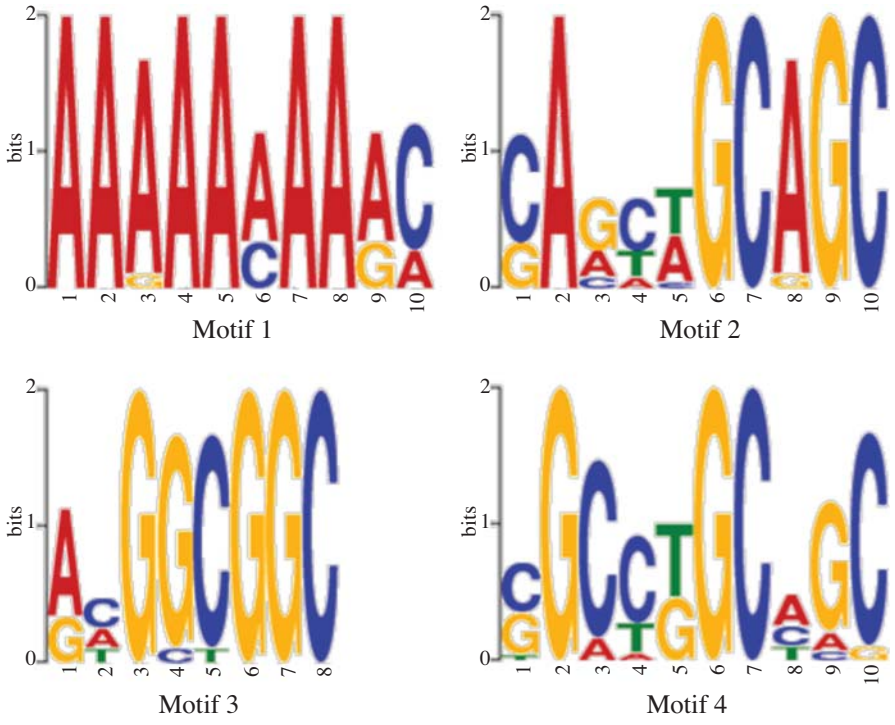

Fig. 23.4 Sequence LOGOS of the MEME motifs 1–4 displaying the probability of each base appearing at every possible position in the motif. The total height of the stack is the information content of that position in the motif in bits. The height of the individual letters in a stack is the probability of the letter at that position multiplied by the total information content of the stack.

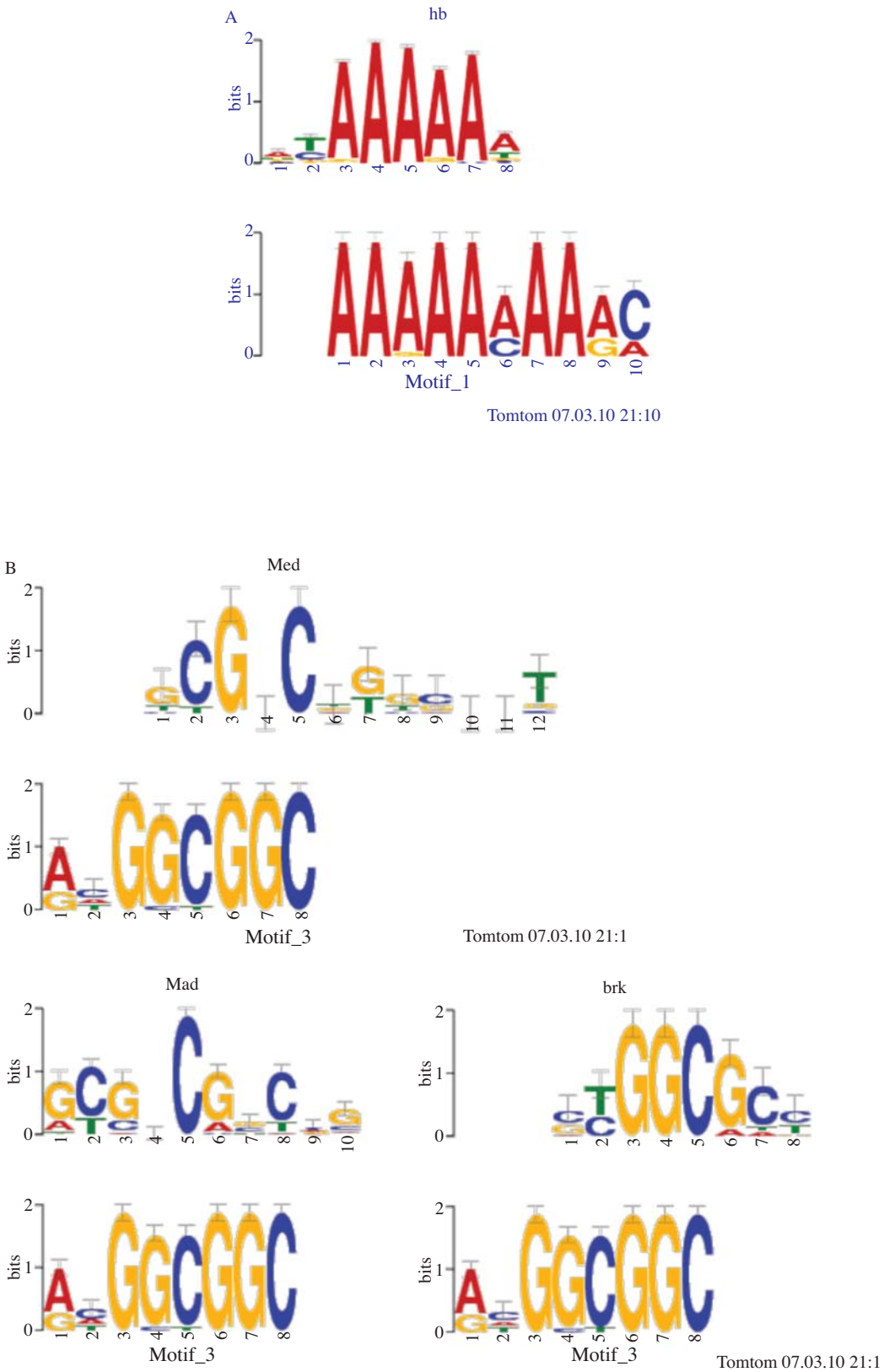

Fig. 23.5 TOMTOM output of the comparison of MEME motifs with existing motifs in the *Drosophila* database (FLYREG; Bergman and Pollard v2). Only statistically significant matches are displayed ($P < 0.001$) with a low false discovery rate ($q < 0.5$). (A) Motif 1. (B) Motif 3. (C) Motif 4.

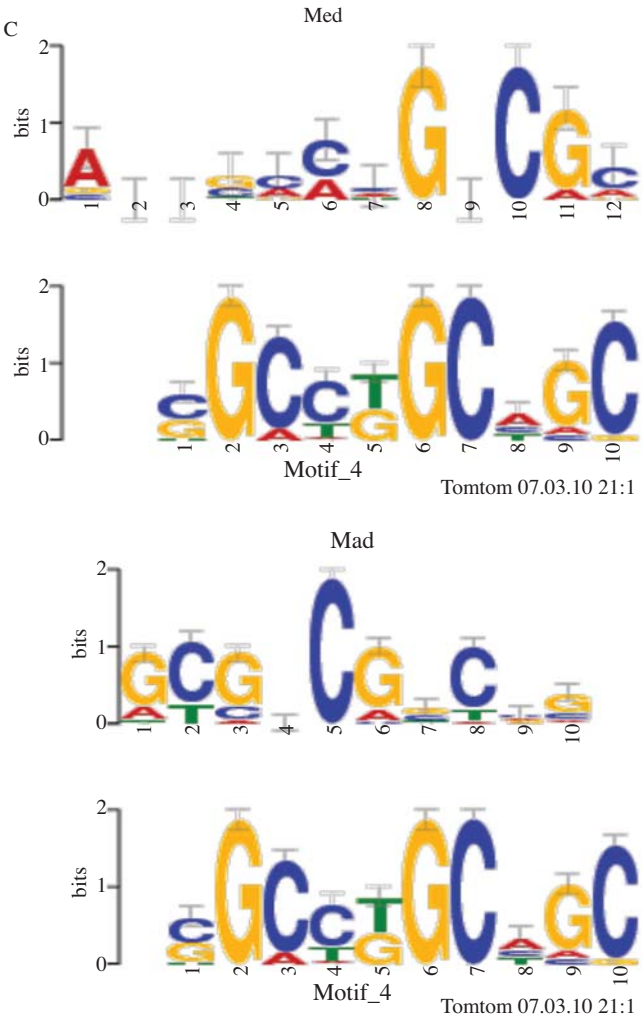

Fig. 23.5 (*Continued*)

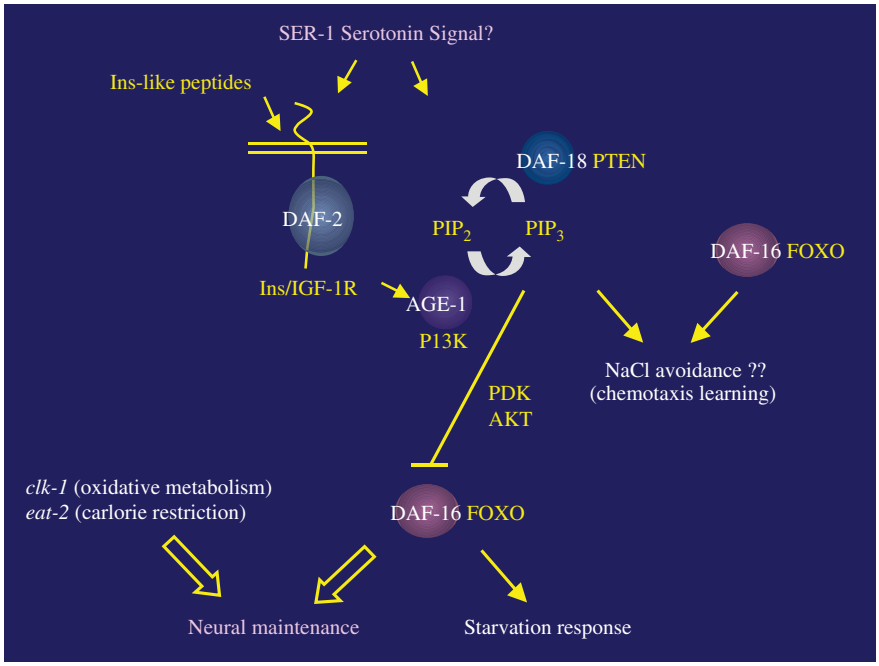

Fig. 25.3 A model for memory regulation by the insulin/IGF-1 pathway. It appears likely that the effects of life extension, or improved neuronal maintenance, lead to an increase in temperature-food association.

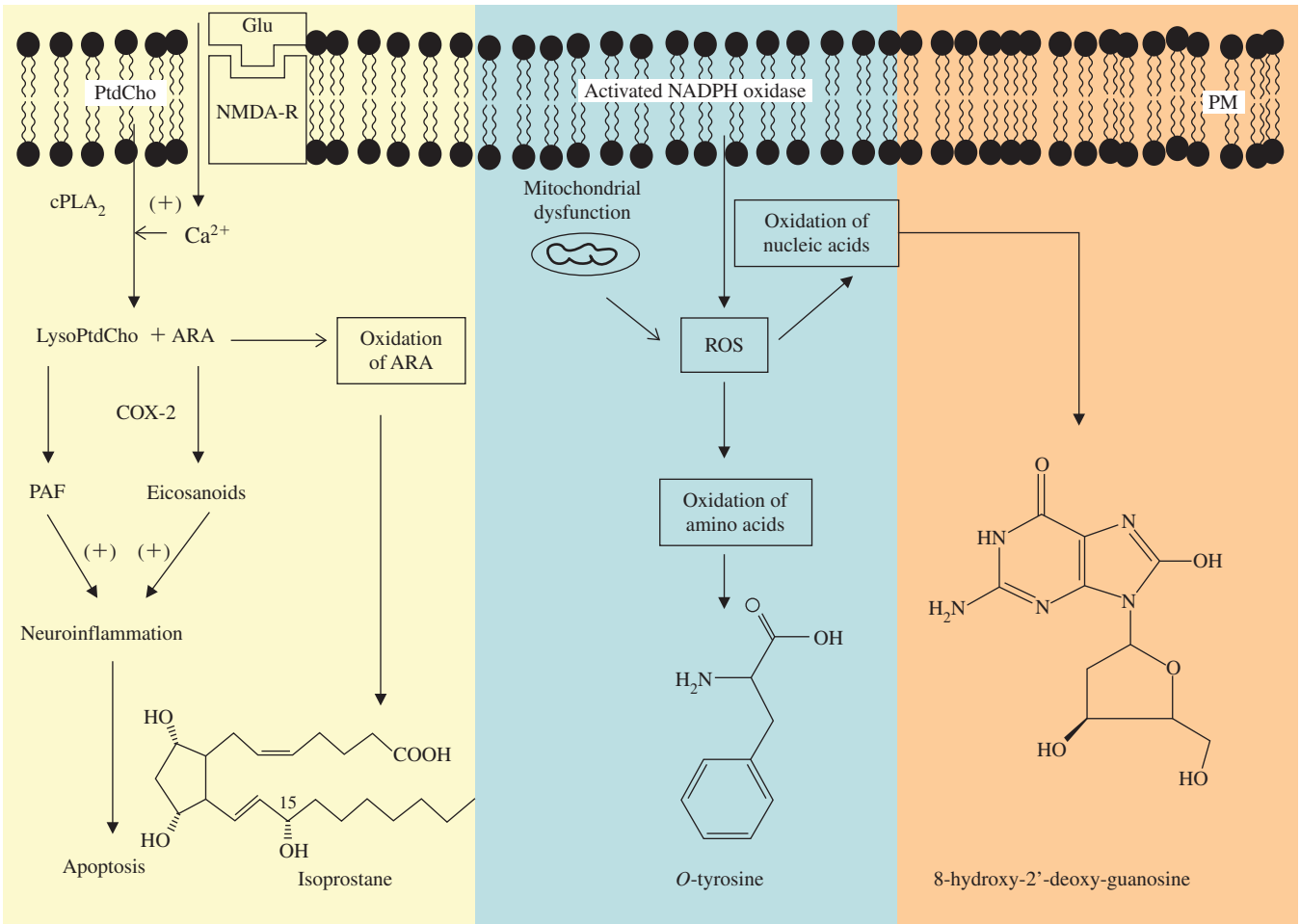

Fig. 27.2 Generation of biomarkers for oxidative stress in vertebrates. PM, plasma membrane; NMDA-R, *N*-methyl-D-aspartate receptor; Glu, glutamate; PtdCho, phosphatidylcholine; lyso-PtdCho, lyso-phosphatidylcholine; $cPLA_2$, cytosolic phospholipase A_2; COX-2, cyclooxygenase; ARA; arachidonic acid; PAF, platelet-activating factor; ROS, reactive oxygen species.